

2006

A Geophysical Interpretation of the Secular Displacement and Gravity Rates Observed at Ny-Ålesund, Svalbard in the Arctic— Effects of Post-Glacial Rebound and Present-Day Ice Melting

Tadahiro Sato

Jun'ichi Okuno

Jacques Hinderer

Daniel S. MacMillan

Hans-Peter Plag
Old Dominion University

See next page for additional authors

Follow this and additional works at: https://digitalcommons.odu.edu/ccpo_pubs

Repository Citation

Sato, Tadahiro; Okuno, Jun'ichi; Hinderer, Jacques; MacMillan, Daniel S.; Plag, Hans-Peter; Francis, Olivier; Falk, Reinhard; and Fukuda, Yoichi, "A Geophysical Interpretation of the Secular Displacement and Gravity Rates Observed at Ny-Ålesund, Svalbard in the Arctic— Effects of Post-Glacial Rebound and Present-Day Ice Melting" (2006). *CCPO Publications*. 49.
https://digitalcommons.odu.edu/ccpo_pubs/49

Original Publication Citation

Sato, T., Okuno, J., Hinderer, J., MacMillan, D. S., Plag, H.-P., Francis, O., Falk, R. and Fukuda, Y. (2006). A geophysical interpretation of the secular displacement and gravity rates observed at Ny-Ålesund, Svalbard in the Arctic: Effects of post-glacial rebound and present-day ice melting. *Geophysical Journal International*, 165: 729–743. doi: 10.1111/j.1365-246X.2006.02992.x

Authors

Tadahiro Sato, Jun'ichi Okuno, Jacques Hinderer, Daniel S. MacMillan, Hans-Peter Plag, Olivier Francis, Reinhard Falk, and Yoichi Fukuda

A geophysical interpretation of the secular displacement and gravity rates observed at Ny-Ålesund, Svalbard in the Arctic—effects of post-glacial rebound and present-day ice melting

Tadahiro Sato,¹ Jun'ichi Okuno,^{2,*} Jacques Hinderer,³ Daniel S. MacMillan,⁴ Hans-Peter Plag,^{5,†} Olivier Francis^{6,‡} Reinhard Falk⁷ and Yoichi Fukuda²

¹National Astronomical Observatory of Japan, 2-12 Hoshigaoka, Mizusawa, 023-0861, Japan. E-mail: tsato@miz.nao.ac.jp

²Kyoto University, Oiwake-cho, Kitashirakawa, Sakyo-ku, Kyoto, 606-8224 Japan

³Institut de Physique du Globe de Strasbourg (UMR 7516 CNRS/ULP) 5 rue René Descartes, F-67084 Strasbourg Cedex, France

⁴NVI, Inc./NASA Goddard Space Flight Center, Greenbelt, Md. 20771-0001, USA

⁵Norway Mapping Authority, N-3511, Hønefoss, Norway

⁶European Center for Geodynamics and Seismology, 19, rue Josy Welter, L-7256, Luxembourg

⁷Bundesamt für Kartographie und Geodäsie, Richard-Strauss-Alle 11, D-60598, Frankfurt am Main, Germany

Accepted 2006 March 6. Received 2006 March 4; in original form 2004 October 13

SUMMARY

We have analysed the Ny-Ålesund very long baseline interferometry (VLBI) data over the period 1994 August to 2004 May, and we obtain secular displacement rates relative to a NNR-NUVEL-1A reference frame of $0.2 \pm 0.5 \text{ mm yr}^{-1}$, $-1.7 \pm 0.5 \text{ mm yr}^{-1}$ and $4.8 \pm 1.1 \text{ mm yr}^{-1}$ for the north, east and vertical directions, respectively. The corresponding global positioning system (GPS) station displacement rates relative to the same reference frame for the north, east, and vertical directions are $0.2 \pm 0.6 \text{ mm yr}^{-1}$, $-2.3 \pm 0.6 \text{ mm yr}^{-1}$, and $6.4 \pm 1.5 \text{ mm yr}^{-1}$ at NYA1 and $-0.1 \pm 0.5 \text{ mm yr}^{-1}$, $-1.6 \pm 0.5 \text{ mm yr}^{-1}$, and $6.9 \pm 0.9 \text{ mm yr}^{-1}$ at NALL, where these GPS rates were derived from the ITRF2000 velocity solution of Heflin. From the comparison at 25 globally distributed collocated sites, we found that the difference in uplift rate between VLBI and GPS at Ny-Ålesund is mainly due to a GPS reference frame scale rate error corresponding to 1.6 mm yr^{-1} in the GPS vertical rates. The uplift rate was estimated to be $5.2 \pm 0.3 \text{ mm yr}^{-1}$ from the analysis of the tide gauge data at Ny-Ålesund. Hence the uplift rates obtained from three different kinds of data are very consistent each other. The absolute gravity (AG) measurements at Ny-Ålesund, which were carried out four times (period: 1998–2002) by three different FG5 absolute gravimeters, lead to a decreasing secular rate of $-2.5 \pm 0.9 \mu\text{Gal yr}^{-1}$ ($1 \mu\text{Gal} = 10^{-8} \text{ m s}^{-2}$). In this analysis, the actual data obtained from a superconducting gravimeter at Ny-Ålesund were used in the corrections for the gravity tide (including the ocean tide effect) and for the air pressure effect. We have estimated three geophysical contributions to examine the observed rates: (1) the effect of the sea-level (SL) change on a timescale of a few decades, (2) the effect of the present-day ice melting (PDIM) in Svalbard and (3) the sensitivity of the computed post-glacial rebound (PGR) effects to different choices of the models of past ice history and Earth's viscosity parameters. Our analysis indicates that the effect of SL change can be neglected as the main source of the discrepancy. On the other hand, the effect of PDIM cannot be ignored in explaining the mutual relation between the observed horizontal and vertical rates and the predicted ones. A large melting rate of the order of -75 cm yr^{-1} (i.e. roughly 1.6 times larger than the mean rate derived from glaciology over Svalbard) would explain the observed uplift but only half of the gravity changes. Our comparison results clearly point out the importance of both the estimation accuracy of the elastic deformations and better observation accuracy to constrain the size of PGR effects in the northwestern Svalbard more tightly.

*Now at: Earthquake Research Institute, University of Tokyo, 1-1-1 Yayoi, Bunkyo-ku, Tokyo, 113-0032, Japan.

†Now at: University of Nevada, Reno, Reno, Nevada 89557-0088, USA.

‡Now at: University of Luxembourg, 162a, avenue de la Fancerie, L-1511, Luxembourg.

Key words: geodetic observations, Ny-Ålesund, post-glacial rebound, present-day ice melting, sea-level change.

1 INTRODUCTION

It is known that northern Europe and the Arctic region have experienced crustal deformation due to the effect of post-glacial rebound (PGR), which is the response of the Earth to the mass redistributions associated with the glacial cycles in the Late Pleistocene. In the study of PGR, the observed secular rates at Ny-Ålesund, Svalbard should give us a useful constraint for the geophysical processes related to PGR, because of the unique capabilities of the high-latitude observation station at Ny-Ålesund (i.e. 79°N in latitude) where several kinds of space geodetic observations are collocated (Plag 1999). In addition to displacement measurements, episodic absolute gravity (AG) measurements have been conducted at Ny-Ålesund since 1998 by several institutes in Europe with FG5 absolute gravimeters. Temporal gravity changes are driven in two ways: that is, the vertical crustal motion and the redistribution of the mass above and/or within the Earth. Thus the gravity measurements offer an independent control for the secular height changes deduced from space-geodetic measurements. Moreover, since 1999 September, the Norwegian Mapping Authority (NMA) and the National Astronomical Observatory, Japan have conducted continuous gravity observations with a superconducting gravimeter (SG) under the framework of GGP (Global Geodynamics Project, Crossley *et al.* 1999). The SG data will give us reliable corrections for the AG measurements.

As will be shown later, the observed uplift rates are about two times larger than many of the proposed model results for the PGR effect, which predict that the crust in the vicinity of Ny-Ålesund is uplifting at a rate of no more than 2–3 mm yr⁻¹ (for example, Lambeck 1995; Kaufmann & Wolf 1996; Kaufmann & Wu 1998; Scherneck *et al.* 2002). Usually, it is difficult to separate the uplift rate due to the long-term viscous response of the Earth by only using displacement observations or gravity observations, because the two effects (the elastic and viscous deformations) are mixed in the observed data. Related to this problem, Wahr *et al.* (1995) demonstrated a method to separate the viscous contribution from the observed data by collocating the position and gravity measurements. Therefore, by combining the observed data from global positioning system (GPS) and/or VLBI and AG, we have an opportunity to discuss the elastic and viscous problems separately (van Dam *et al.* 2000; Larson & van Dam 2000).

In order to be able to discuss PGR more thoroughly, it is important to increase the accuracy of computation of the elastic effects. Among the elastic effects, we considered here the effects of sea-level (SL) changes and present-day ice melting (PDIM). Radio echo-sounding data indicate that the mean thickness averaged over all major glaciers of Svalbard is close to 200 m (Macheret *et al.* 1985). Our preliminary computation using a simple glacier model, which uniformly covers Svalbard with a 200-m-thickness layer, suggests that the PDIM effect is about 2.3 mm yr⁻¹ for the uplift of the ground and $-0.4 \mu\text{Gal yr}^{-1}$ for the gravity change when the glacier is melting at a rate of about 50 cm yr⁻¹. As will be shown later, these effects cannot be ignored in the comparison with the observations.

This paper consists of two parts. The first is a discussion of the observed displacement and gravity rates at Ny-Ålesund and the second is on the model computations and the comparison between the observations and the models. Related to the PGR effect, we will also discuss the regional displacement rate in the Kings Bay area based

on two data sets. One is the tide gauge data at Ny-Ålesund and the other one is the data from the GPS campaigns that NMA has carried out in the Kings Bay area (Bockmann *et al.* 2002). Finally, we will discuss the sensitivity of the computed PGR effects to the proposed ice models and the combination of Earth's viscous parameters that are optimal in explaining the mutual relation among the observed vertical and horizontal displacement rates and the gravity rate. For the sign convention, we use here a positive sign for the northward, eastward and upward displacements and the increase of gravity (i.e. increase of the downward force).

Fig. 1 shows the location of Ny-Ålesund together with the observation facilities related to this paper.

2 DATA ANALYSIS

2.1 Displacement rates

2.1.1 Rates obtained from continuous VLBI and GPS measurements

NMA regularly monitors the position of Ny-Ålesund with collocated VLBI and GPS stations that participate in the determination of the ITRF system (International Terrestrial Reference Frame, Altamimi *et al.* 2002). For VLBI, we performed a terrestrial reference frame solution using all VLBI observations from the period of 1979–2004. The paper by Ma *et al.* (1990) describes the VLBI least-squares estimation program (SOLVE) that was used for the analysis.

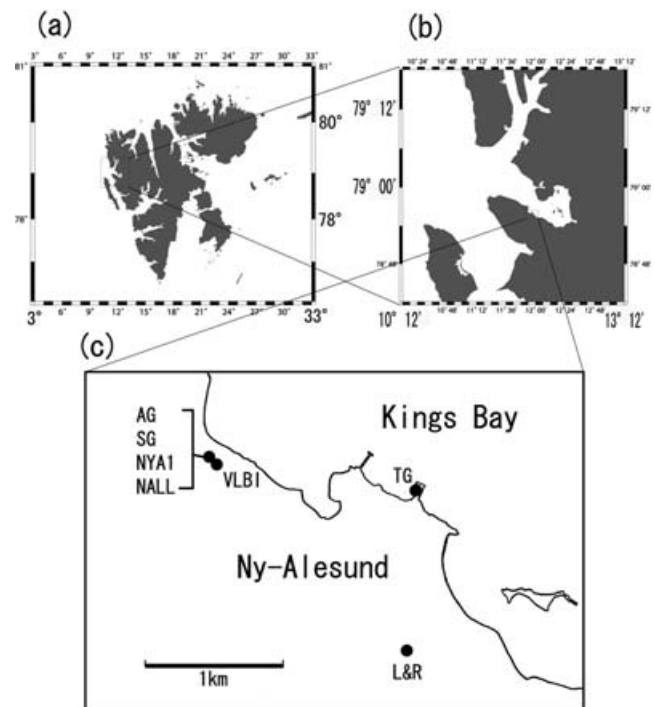


Figure 1. Location map of Ny-Ålesund and the related observation facilities. AG: Absolute Gravimeter, SG: Superconducting Gravimeter, NALL and NYA1: continuous GPS sites, VLBI: VLBI site, TG: Tide Gauge and L&R: LaCoste & Romberg Gravimeter.

For the theoretical models, we followed the IERS 1996 Convention (McCarthy 1996). In this type of solution, station positions, station velocities and radio source positions are estimated from all the data. Here, the station positions and velocities were aligned to ITRF2000 (Altamimi *et al.* 2002) via no net translation and rotation constraints on the positions and velocities of the 12 most frequently observed globally distributed VLBI rigid plate sites. Only the horizontal adjustments were constrained in the translation constraint. Similarly, radio source positions were aligned to *a priori* ICRF (International Celestial Reference Frame) positions with a no net rotation constraint. In this solution, there were 448 VLBI observing days at Ny-Ålesund over the period 1994 August to 2004 May. For comparisons between observed geodetic rates and model displacement rates at Ny-Ålesund, we want the velocity of Ny-Ålesund relative to the rigid European plate. To approximate this, we performed another solution with the velocities estimated relative to the NNR-NUVEL-1A plate model (De Mets *et al.* 1994) velocities of the 12 sites at rigid plate locations. The velocities from these solutions are shown in Table 1.

For GPS, we used the velocities from the standard operational GPS solution made by NASA JPL (Jet Propulsion Laboratory) using the data obtained from the global world wide GPS networks (Heflin 2004). In the standard JPL solution, the positions are transformed to the ITRF2000 reference frame each day by applying a seven-parameter Helmert transformation, where the seven parameters are the three components of the geocentre vector offset, three rotation parameters and a reference frame scale parameter (Heflin, personal communication, 2004). For Ny-Ålesund, we used the velocities of the two continuously observing GPS receivers, that is, NALL and NYA1 (see Fig. 1). NYA1 is located on the same pier with the SG and NALL is located 6.5 m away from NYA1 horizontally. The JPL GPS solution includes the observations from 1998 March to 2004 February at NYA1 and from 1991 January to 2004 February at NALL. To obtain the horizontal velocities in the NNR-NUVEL-1A frame, we determined a six-parameter (translation plus rotation) transformation between the GPS velocities and the NNR-NUVEL-1A velocities using a reference set of 39 sites on rigid plates. This was a subset of the GPS sites used by Altamimi *et al.* (2002) in the definition of ITRF2000. Sites with horizontal velocity residuals (relative to NUVEL1A-NNR) greater than 4 mm yr^{-1} were removed from the list of reference sites.

In both the ITRF2000 and NNR-NUVEL-1A frames, comparison of the GPS and VLBI horizontal velocities shows that they agree within their formal uncertainties. However, usually, the formal uncertainties taken directly from the analysis solutions are unrealistically small, since they are dominated by the effect of $1/\sqrt{N}$ where

Table 1. Secular displacement rates at Ny-Ålesund obtained from the VLBI and GPS data and the regional displacement rates. The first line for the VLBI and GPS (Heflin 2004) indicates rates given in an ITRF2000 frame. The second line indicates rates in a NNR-NUVEL-1A frame. The values in parentheses show the observation errors.

	NS (mm yr^{-1})	EW (mm yr^{-1})	Vertical (mm yr^{-1})
VLBI	14.4 (0.5)	10.3 (0.5)	5.1 (1.1)
	13.8	11.3	4.8
GPS (NYA1)	14.6 (0.6)	10.0 (0.6)	6.6 (1.5)
	13.8	10.7	6.4
GPS (NALL)	14.2 (0.5)	10.7 (0.5)	7.0 (0.9)
	13.5	11.4	6.9
NUVEL1A-NNR	13.6	13.0	—

N is the number of observing days. To account for this, we have for simplicity used the method of Argus & Gordon (1996) that adds an upper bound error term $\Delta x/T$ in quadrature to the horizontal formal uncertainties, where T is the observing period in years. In the analysis of North American VLBI velocities located in the most stable part of the plate, we found that $\Delta x = 3 \text{ mm}$ was required to be statistically consistent with plate rigidity. Since for most sites, vertical formal uncertainties are about 3 times as large as that of the horizontal components, we used $\Delta x = 9 \text{ mm}$ here for the vertical uncertainty correction. Tests that we have done in which the set of reference sites was modified to determine the effect on estimated velocities led to a level of reference frame rms uncertainty of $0.3\text{--}0.4 \text{ mm yr}^{-1}$ in the vertical, east, and north components. Based on this, we added 0.4 mm yr^{-1} in quadrature to the horizontal uncertainties for both the VLBI and GPS velocities to account for reference frame error. The errors shown in Table 1 were obtained in this way.

2.1.2 Reference frame scale rate error in GPS

As shown in Table 1, while two different techniques (VLBI and GPS) give consistent rates for the horizontal components, the vertical rates obtained from the GPS measurements are larger than that from VLBI by 1.6 mm yr^{-1} to 2.1 mm yr^{-1} . Compared with the observation errors, this difference is significant. Related to this, we point out that Steinforth *et al.* (2003) examined the stability of the geodetic reference point of the VLBI antenna by comparing the results of two local survey campaigns carried out in 2000 and 2002 with a trigonometric method. They found that the geodetic reference point of the VLBI antenna itself was stable over the 2 yr period to within $-0.3 \pm 0.6 \text{ mm}$, $-0.8 \pm 0.3 \text{ mm}$, $0.0 \pm 0.8 \text{ mm}$ in the vertical, EW, and NS directions, respectively (see their Table 2).

We have investigated the possibility that the origin of this discrepancy is a rate difference between the VLBI and GPS reference frame scales (MacMillan 2004). In other words, if we measure the vector \mathbf{r} between any two points at time t , there will be a difference in the coordinate measurements in the two frames that scales as $\alpha(t)\mathbf{r}$ for all \mathbf{r} . The scale rate of change is just the linear rate of change of the parameter $\alpha(t)$. A scale rate difference could arise from modelling errors or differences between the models used in the GPS and VLBI analyses. VLBI is capable of accurately determining scale because of its tie to the extragalactic radio reference positions. Because of this, the ITRF2000 scale is mainly determined by VLBI and SLR (Satellite Laser Ranging) (Altamimi *et al.* 2002).

We considered a set of 25 collocated global GPS and VLBI sites. The vertical GPS rates at 21 of these sites are greater than the corresponding VLBI rates. Performing a seven-parameter transformation between the GPS and VLBI velocities at these collocated sites

Table 2. Summary of absolute gravity observations for Ny-Ålesund during the period 1998–2002. The values are differences with respect to the constant factor of $983\,017\,000 \mu\text{Gal}$ and the errors are 1-sigma formal errors.

Year	Organization	Value μGal	Error μGal
1998	BKG	60.5	0.6
2000	EOST	55.8	6.1
2001	BKG	52.2	1.1
2002	ECGS	51.0	1.6

Note:

BKG: Bundesamt fuer Kartographie and Geodaesie, Frankfurt, Germany.
 EOST: Ecole et Observatoire des Sciences de la Terre, Strasbourg, France.
 ECGS: European Center for Geodynamics and Seismology, Luxembourg.

yielded a scale rate difference of 0.19 ± 0.01 ppb yr^{-1} . To avoid rotation and translation dependences and sensitivities to reference site global distribution, we also examined the baseline length rates from the two techniques. Baseline length series were computed using the same VLBI and GPS epochs. We found that the GPS baseline length rates were greater than the corresponding VLBI baseline length rates by an average of 0.25 ± 0.01 ppb yr^{-1} . Multiplying by the Earth's radius gives a systematic vertical rate difference of 1.6 mm yr^{-1} . This vertical rate difference is close to the difference between the observed VLBI and GPS vertical rates at Ny-Ålesund shown in Table 1.

2.1.3 Rate from the GPS campaign measurements

Since 1998, NMA has carried out GPS campaign measurements in the Kings Bay area Bockmann *et al.* (2002). The total area covered with the campaigns is 50 by 30 km around Ny-Ålesund. Nine monuments including the permanent GPS sites of NALL and NYA1 are set in the area shown in Fig. 1(b). Bockmann *et al.* (2002) recompiled the campaign data by adding the new data set and analysing them with an improved data processing method.

To obtain an idea of the regional displacement rates in the Kings Bay area, if we take the weighted mean over the nine monuments with their observation errors as weights, then we obtain 14.6 ± 0.3 mm yr^{-1} , 10.2 ± 0.4 mm yr^{-1} and 6.6 ± 1.0 mm yr^{-1} for the NS, EW and vertical components, respectively. Comparing rates in Table 1, it is noticeable that the regional mean uplift rate is close to the vertical rate obtained from the continuous GPS observation at Ny-Ålesund discussed above, while the horizontal displacement rates are consistent with the continuous observations at Ny-Ålesund from VLBI and GPS.

2.2 Rate from the tide gauge data

Another data source that we can use to see the vertical rate at Ny-Ålesund is the tide gauge data. In general, tide gauges measure SL changes relative to a benchmark fixed to the ground, thus they measure the changes in the difference between the geocentric sea

level (GSL) and the geocentric height of the benchmark. Therefore, the vertical crustal motion may be represented by the difference—(SL – GSL). Ideally, GSL represents the global SL change due to the change in the ocean mass, and it should be subtracted from the tide gauge data to remove the effect of local crustal motion. Douglas (1997) estimated the magnitude of GSL change using a large number of tide gauge data in the world and correcting for the PGR effect based on the ICE-3G model (Tushingham & Peltier 1991), and he obtained a rate between 1.8 mm yr^{-1} and 1.9 mm yr^{-1} . The error is estimated to be of the order of ± 0.1 mm yr^{-1} . Lambeck *et al.* (1998), who analysed many tide gauges around Fennoscandia, gave 1.1 ± 0.2 mm yr^{-1} as an averaged value for the eustatic SL rise for the past century, which is slightly lower than the value from Douglas (1997).

As will be described in Section 2.4, our analysis results for the tide gauge data indicate that the secular rate of SL changes at Ny-Ålesund is of the order of -3.5 ± 0.3 mm yr^{-1} (see Table 3). If we tentatively assume 1.7 ± 0.2 mm yr^{-1} (i.e. the weighted mean of 1.9 mm yr^{-1} and 1.1 mm yr^{-1}) as the rate of the GSL change, then we obtain a rate of 5.2 ± 0.3 mm yr^{-1} for the uplift rate at Ny-Ålesund. We see that the tide gauge gives a similar rate to the one obtained from VLBI (i.e. 4.8 mm yr^{-1}) rather than the GPS observations including the GPS campaigns. However, the three independent observation techniques give a consistent uplift rate of about 5 mm yr^{-1} , if we correct the GPS observed rates for the scale rate error of 1.6 mm yr^{-1} .

2.3 Gravity rate

2.3.1 Data analysis

During the 5 yr period of 1998–2002, AG measurements have been undertaken four times at the same observation pier of the SG. All AG observations were performed with FG5 absolute gravimeters, though three different instruments were used. The observations were carried out at the same position on the observation pier and always in the summer season. Each observation was more than 1 week in length and the data were processed using the ‘g’ software developed

Table 3. Analysis results for the PSMSL monthly sea level data. The data length used in the analysis is shown in Table 3. The air pressure effect was corrected.

Site	Linear (mm yr^{-1})	Annual		Semi-annual	
		Amp. (mm)	Phs.* (deg)	Amp. (mm)	Phs* (deg)
Torshavn	1.2 (0.1)	55.8 (4.7)	−104.2 (4.8)	13.1 (4.7)	−27.2 (20.6)
Ratan	−8.4 (1.0)	86.6 (9.9)	−59.0 (6.7)	40.3 (9.9)	59.3 (13.3)
Reykjavik	2.2 (0.2)	56.6 (5.5)	−103.3 (5.5)	18.2 (5.5)	−44.0 (24.1)
Ammassalik	2.8 (2.3)	95.2 (9.0)	−26.7 (5.5)	9.4 (9.9)	−136.6 (54.6)
Murmansk	2.3 (7.9)	71.7 (6.9)	−55.8 (5.5)	16.6 (6.9)	−27.2 (23.9)
Tromso	−1.1 (0.2)	82.0 (6.5)	−39.4 (18.6)	18.6 (6.5)	−8.5 (21.1)
Prudhoe Bay	1.6 (6.4)	68.5 (9.1)	−66.4 (7.6)	49.9 (9.1)	−140.4 (10.5)
Jan Mayen	0.2 (1.8)	69.5 (8.9)	−95.6 (7.4)	20.8 (9.0)	12.2 (24.7)
Honningsvåg	1.9 (0.3)	73.9 (6.2)	−45.6 (4.8)	20.4 (6.2)	−7.4 (17.3)
Resolute	−3.8 (0.6)	47.4 (6.7)	−97.3 (8.2)	17.2 (6.8)	22.2 (22.4)
Weighted mean**	0.4 (1.0)	68.7 (7.6)	−70.4 (6.4)	21.1 (7.0)	−29.4 (23.3)
Barentsburg	−3.3 (0.2)	55.8 (5.7)	−82.4 (5.9)	17.8 (5.7)	−8.2 (18.4)
Ny-Ålesund	−3.5 (0.3)	54.6 (6.1)	−88.0 (6.9)	21.6 (6.2)	−13.3 (16.4)
Weighted mean	−3.4 (0.3)	55.2 (5.9)	−85.0 (6.4)	19.6 (5.9)	−10.9 (17.4)

Note:

*Phase: referred to 1997 January 1 as an epoch of analysis.

**Weight: reciprocal of the angular distance from Ny-Ålesund.

by Micro-g and the final gravity values were evaluated by applying the same geophysical correction parameters obtained from the actual observations.

Four geophysical corrections were applied:

- (i) the vertical gravity gradient,
- (ii) the polar motion,
- (iii) the tides including the effect of ocean tide and
- (iv) the atmospheric pressure changes.

The first one is needed to reduce the gravity values to the same height of the observation pier. For this, we used $-0.3594 \mu\text{Gal mm}^{-1}$, which is the mean of the gravity gradient measurements taken in 1998 ($-0.3617 \pm 0.003 \mu\text{Gal mm}^{-1}$) and in 2000 ($-0.3570 \pm 0.003 \mu\text{Gal mm}^{-1}$). The polar motion effect was estimated using the formulation of Wahr (1985) and a nominal value for the gravimetric factor, that is, 1.16. The polar motion data were taken from the daily values available at the International Earth Rotation Service (IERS).

While the oceanic tide effect at Ny-Alesund is as large as 1.4 times the body tide effect especially in the semi-diurnal frequencies (Sato *et al.* 2003), it change substantially as a function of the distance from the coast (Bos *et al.* 2002). Therefore, we used the actual gravity tides obtained from the SG data for this correction, from the analysis of 3 yr (1999 September-2002 August) of data. For the Sa (annual) and Ssa (semi-annual) waves, we corrected their effects by simply assuming the values of 1.16 and 0.0 degree as the gravimetric δ -factor and phase, because the errors for these waves are still large. By using a tidal analysis code 'BAYTAP-G' (Tamura *et al.* 1991), the tidal parameters were determined simultaneously with the admittance of the gravity data to the local air pressure changes. The admittances obtained from successively yearly analysis change in amplitude within a range between -0.32 and $-0.45 \mu\text{Gal hPa}^{-1}$. We adopted here a value $-0.417 \pm 0.004 \mu\text{Gal hPa}^{-1}$, which was derived from the analysis for the 3 yr of data.

Table 2 shows the results for the AG measurements with their $1-\sigma$ formal errors. The observations in 2000 show a large error of $\pm 6.1 \mu\text{Gal}$. This is related to the fact that the instrument superspring was malfunctioning during that period in addition to bad weather conditions during the observation. A similar but much more serious accident occurred in 2002 during the transportation of the absolute gravimeter from Greenland to Svalbard. At that time, the string fixing the superspring to the frame was repaired temporarily. Despite this temporary repair, the observation error in 2002 is not larger compared with those in other years thanks to good weather conditions.

2.3.2 Error estimation

We have investigated the sensitivity of the correction parameters by using different model parameters in the data processing. For example, for the tide that is the largest correction in our case, we find that if instead of using the observed tidal parameters determined from the actual SG data, a nominal earth tide and ocean loading model is used, the mean value of gravity can differ by up to $1 \mu\text{Gal}$. Moreover, we have also confirmed that, compared with the results obtained using the default tide and pressure admittance value (i.e. $-0.3 \mu\text{Gal hPa}^{-1}$) installed in the data processing package of Micro-g, the standard error of the estimated AG value has been improved by about 150 per cent (from $\pm 0.2 \mu\text{Gal}$ to $\pm 0.14 \mu\text{Gal}$) by using the observed parameters for the tide and air pressure changes. This revision in the error clearly indicates the advantage of using the tide and air pressure corrections based on the actual measurements at the

observation site. We have also tested the sensitivity to the gravity gradient, and we found that changing the gradient by $0.04 \mu\text{Gal cm}^{-1}$ (the difference between the 1998 and 2000 determinations) can change the mean value of gravity by $0.2 \mu\text{Gal}$.

From the tests mentioned above, the systematic error in our analysis for the AG data due to the error of the corrections is of the order of $\pm 0.3 (= 0.14+0.2) \mu\text{Gal}$. Compared with the observation errors shown in Table 2 obtained from the AG data analysis, this error is small enough. However, similarly to the case of the analysis of displacement data, in general the $1-\sigma$ formal error usually underestimates the true uncertainty, because it ignores a systematic error mainly due to an offset between the instruments (e.g. Francis *et al.* 1999). For example, according to the results of an intercomparison measurement campaign conducted at the BIPM in Sevres, Paris, France with seven different FG5 gravimeters (Robertsson *et al.* 2001), the FG5 determinations of gravity have a rms error of approximately $2 \mu\text{Gal}$. This means that observing gravity changes in Ny-Ålesund with different FG5s may introduce an uncertainty at this level to each observation. If we add $2 \mu\text{Gal}$ in quadrature to all the formal errors determined in the data processing and we fit a line using the new errors as a weight, then we finally obtain a value of $-2.5 \pm 0.9 \mu\text{Gal yr}^{-1}$ as our best estimate for the secular gravity rate at Ny-Ålesund. Fig. 2 shows the AG data and the best fitting line taking these errors into account.

2.4 Analysis of the SL changes

2.4.1 Data and analysis

To obtain a spatial field of SL changes to be used in the computation of the attraction and loading effects due to the SL changes, we have analysed the data at 12 tide gauge stations in the northern Atlantic Ocean and the seas of the polar region located at more than 60°N in latitude. Data used here are the monthly data archived at the Permanent Service for Mean Sea Level (PSMSL) of Proudman Oceanographic Laboratory of United Kingdom (<http://www.pol.ac.uk/psmsl/>, Woodworth 1991; Woodworth *et al.* 1999). Table 4 shows the tide gauge stations used in this study. Except for Jan-Mayen, data more than 20 yr in length are available for these stations. Although the data length of Jan-Mayen is short (i.e. 11 yr), we included it in our analysis, because it is located at almost the centre of the Greenland

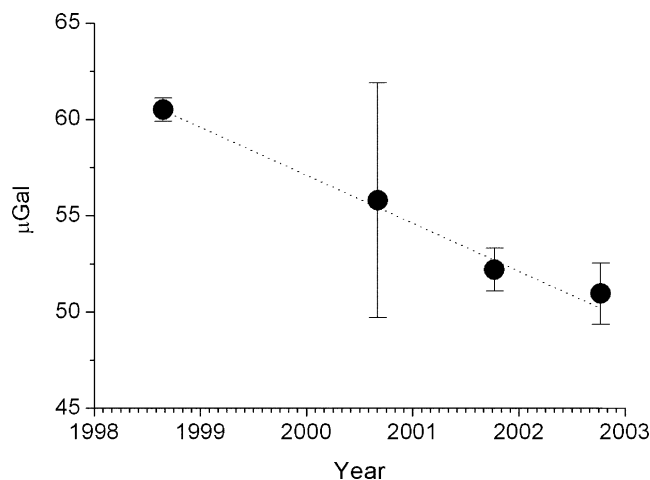


Figure 2. Plot of the absolute gravity values shown in Table 2 and the best fitted line.

Table 4. List of the tide gauge stations and analysis period used in this study.

Station	Code	Latitude(N)	Longitude(E)	Analysis period
Torshavn	015011	62.017	353.233	1957–2000
Ratan	050191	64.000	20.917	1892–2000
Reykjavik	010001	64.150	338.067	1951–2000
Ammassalik	980071	65.500	323.000	1990–1999
Murmansk	030018	68.967	33.050	1952–2000
Tromso	040031	69.650	18.967	1952–2000
Prudhoe Bay	821002	70.417	211.467	1994–2000
Jan-Mayen	012001	70.917	351.283	1974–1983
Honningsvag	040015	70.983	25.983	1970–2000
Resolute	970151	74.683	265.117	1957–1977
Barentsburg	025001	78.067	14.250	1948–2000
Ny-Ålesund	025021	78.933	11.933	1976–2000

Sea, and it is useful to see the behaviour of the SL changes at the middle of the related oceans.

The local air pressure changes were corrected by assuming the inverted barometer (IB) response of the ocean to the air pressure changes (i.e. $-10.0 \text{ mm hPa}^{-1}$). For the correction, we used the monthly grid-point data called ‘Grid-Point Pressure Data for the Northern Hemisphere’, which are provided by the Climate Research Unit of University East Anglia of United Kingdom (<http://www.cru.uea.ac.uk/cru>, Basnett & Parker 1997). The resolution of the data is 10° and 5° in longitude and in latitude, respectively. The pressure changes at each tide gauge station were spatially interpolated from the grid data. To assess the quality of interpolated data, we compared the time-series data interpolated at Ny-Ålesund with the actual observational data for the period of 1998–2001. The regression coefficient between the two data sets is 0.846 ± 0.039 and the standard deviation of the differences between the two data sets is 2.0 hPa. The value of 2.0 hPa corresponds to about 10 per cent of the peak-to-peak amplitude of the observed pressure changes during the 4 yr.

The SL data corrected for the air pressure changes were decomposed into four terms (i.e. the constant, linear, annual and semi-annual terms) by means of a least squares method. Table 3 shows the analysis results. In the archives of the PSMSL, the two tide

gauge stations available in Svalbard are Ny-Ålesund and Barentsburg, which is located about 90 km south of Ny-Ålesund. As shown by the four terms in Table 3, these two stations give very consistent SL changes, suggesting a homogenous change in SL around the western Svalbard.

2.4.2 Time dependence of the estimated secular SL rate

The estimated linear rate of SL change depends on the length of tide gauge data used in the analysis and also on the analysis epoch. There are fluctuations of the tide gauge data due to the decadal seesaw-like fluctuations in the weather system called the North Atlantic Oscillation (NAO) (for example, Rodwell *et al.* 1999). Plag & Tsimplis (1999), who analysed many tide gauge data sets in the North Sea and Baltic Sea, pointed out the fluctuations related to NAO. Campbell & Nothnagel (2002) compared the European VLBI results including Ny-Ålesund with the mean SL from tide gauge data, and they also pointed out the effect of the decadal SL changes.

Fig. 3 shows the temporal changes in the estimated secular rate of SL at Ny-Ålesund and Barentsburg. Figs 3(a) and (c) show monthly data from the two tide gauges and their mean rates and Figs 3(b) and (d) show the time variations of the secular rates obtained from successive 5 yr analysis periods centred at each yearly epoch. As shown in Figs 3(b) and (d), for the most recent 5 yr period (1996–2000), the rates are estimated to be $-18 \pm 5 \text{ mm yr}^{-1}$ and $-11 \pm 9 \text{ mm yr}^{-1}$ at Ny-Ålesund and Barentsburg, which are three to five times larger than the rates of -3.5 mm yr^{-1} and -3.3 mm yr^{-1} shown in Table 3.

2.5 Rate of PDIM

Temporal variations in glacier mass balance are regularly monitored at many places in the world, and the results are reported in several data books such as ‘Glacier Mass Balance Bulletin’ (GBB, World Glacier Monitoring Service 2001), ‘Fluctuations of Glaciers’ (FG, World Glacier Monitoring Service 1998) and ‘World Glacier Inventory’ (WGI, World Glacier Monitoring Service 1989). According to these data books, it is obvious that many of the glaciers in

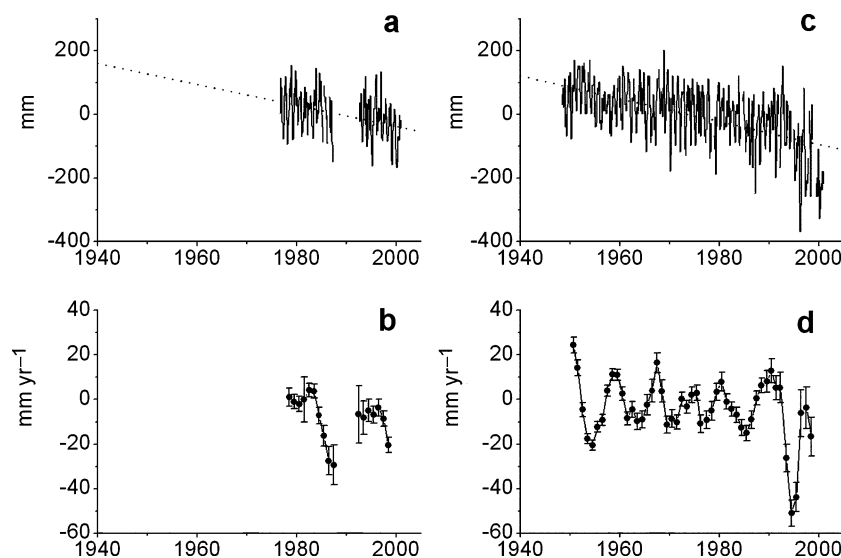


Figure 3. Dependence of the estimated secular rate of SL changes on the data length used for the analysis. The two top plots show the monthly data from the Ny-Ålesund (a) and Barentsburg (c) tide gauges with the fitted curves (dotted line), respectively. The two bottom plots show the time variations of the secular rates for Ny-Ålesund (b) and Barentsburg (d) obtained from successive 5 yr analyses shifting the analysis epoch by 1 yr.

Europe are rapidly decreasing in volume. In Svalbard, four glaciers near Ny-Ålesund are regularly monitored: Austre Broggerbreen (78:30N and 11:50E), Midtre Lovenbreen (78:53N and 12:04E), Hansbreen (77:05N and 15:40E), and Kongsvergen (78:50N and 12:59E). Except for Hansbreen, which is located in the south of Spitsbergen, the other three glaciers are located within a distance of 3–17 km from Ny-Ålesund.

According to the figures shown in Vol. 6 of GBB, the glaciers in Svalbard are melting with a regular rate of -27 cm yr^{-1} to -43 cm yr^{-1} except for Kongsvergen. This glacier shows a large oscillation in mass balance of about 40 cm yr^{-1} in peak-to-peak amplitude with a period of about 6 yr since 1985 when the monitoring started. However, the rate over the period 1995–2000 that overlaps the period of our AG measurements is estimated to be about -33 cm yr^{-1} . If we take a simple mean over the four glaciers during the period of 1995–2000, we obtain a rate of -34 cm yr^{-1} .

Based on the data for the period of 1950–1988, Hagen & Liestol (1990) investigated the long-term glacier mass-balance of five glaciers in Svalbard. The rate of the mean mass balance over the five glaciers given in their Table 2 is -53 cm yr^{-1} , which is much higher than the above value. On the other hand, Dowell *et al.* (1997), who studied the relation between the mass balance of circum-Arctic glaciers and recent climate change, also gives a high rate of -55 cm yr^{-1} as the averaged value over the three glaciers in Svalbard. For our analysis, we take the average of the above estimates, that is, -47 cm yr^{-1} , as the mean melting rate over the Svalbard Archipelago.

3 THEORETICAL MODELLING

3.1 Computation method of the elastic loading effects

Mass changes in the sea and on land affect the observed displacement and gravity changes through the deformation of the ground by loading effects (i.e. the effect of deformation and the change in the direct gravity attraction). According to Farrell (1972) we estimated the effects of SL variations and PDIM by convolving the changing mass with the loading Green's function defined at the solid surface (i.e. at the deformed surface) over the sea or land area considered.

The gravity Green's function consists of three terms:

- (1) the direct gravity Newtonian attraction due to the loading mass,
- (2) the effect of elastic deformation of the Earth in the vertical direction that is represented using load Love number h'_n and
- (3) the effect of density changes inside the Earth that is represented using load Love number k'_n , where n is the order of the spherical harmonic decomposition of the load.

The order up to 10 000 was considered in our computation. The gravity observation made on land is affected by a free-air gravity change with a rate of about $-0.3 \mu\text{Gal mm}^{-1}$. Our computation, which is made on the deformable solid surface, includes the free-air gravity effect through the h'_n term of the Green's function formalism. As described below, the same remark applies to the PGR loading computation, the only difference being in the rheology (elastic for the PDIM and SL changes, viscoelastic for the PGR).

3.2 Effect of SL changes

As suggested by many previous studies of the oceanic tidal loading effects, nearby seas within 20° – 30° in loading distance make the dominant contribution to the convolution integral in the case of

displacement and gravity (about 80–90 per cent of the total effect from summing over all the oceans on the Earth; see for example, Sato & Hanada 1984). As a test to estimate the effect of SL changes, we computed the contributions of two coaxial circular sea areas of 0° to 6° and 6° to 20° in angular distance measured from Ny-Ålesund. We used the weighted means shown in Table 3 of the two stations Ny-Ålesund and Barentsburg for the inner coaxial circular region and those of the remaining 10 stations for the outer coaxial region. In the computation, both the altitude of the observation station and each loading mass are taken into account. The effect of the finite area of each grid mesh (see Farrell 1973) was also considered by applying a formula obtained by analytically integrating the Green's function in the convolution, which was approximated with a second-order polynomial over the rectangular sea mesh (Sato & Hanada 1984).

The Ny-Ålesund site is close to the coast of Kings Bays (see Fig. 1c) and is located at the edge of a steep slope of about 40 m in altitude. This causes the convolution result to be sensitive to the accuracy of the topographic maps used for the land-sea mask, especially for the attraction part of the gravity effect (see Sato *et al.* 2001a, 2003). Thus, to represent precisely the coastal topography in the vicinity of the observation site, a fine grid of $5.0''$ by $7.5''$ in latitude and longitude was used for the area of $45''$ by $67.5''$ around the observation site and the remaining area shown in Fig. 1(b) was represented by using the grid of $1.0'$ by $2.5'$ in size. Outside of this area, we used two different kinds of grids, that is, $5'$ by $5'$ and 1.25° by 1.25° for the areas within less than 30° and greater than 30° , respectively.

Table 5 shows the computation results obtained using the Green's function for the PREM earth model (Dziewonski & Anderson 1981). In this study, we only considered the sea region within 20° in angular distance from Ny-Ålesund. If we assume a secular rate of 1.7 mm yr^{-1} (see Section 2.2) for all the remaining sea regions in the world, for the gravity, the contribution at Ny-Ålesund from the remaining seas is estimated to be about $0.04 \mu\text{Gal yr}^{-1}$ (i.e. sense of the increasing of the gravity), where the gravity contribution is relatively large compared with other components.

3.3 Effect of PDIM

The computation method is similar to that used for the SL changes described in Section 3.1, although, of course, the masking of the sea and land is opposite. The parameters considered here are the following:

- (1) the mean melting rate of the glaciers,
- (2) the 3-D location and area of glaciers,
- (3) the thickness of the glaciers and
- (4) the density of ice.

For (1), we used -47 cm yr^{-1} as explained in Section 2.5. For (2) and (3), we used a similar model to that proposed by Hagedoorn & Wolf (2003) who represented the 3-D distribution of the 16 major glaciers in the four main islands of Svalbard Archipelago with coaxial elliptical cylinders (SVAL model). We adjusted the total area of each glacier model to that given in WGI-1998. For (4), we used the value of 1000 kg m^{-3} , because the magnitude of ice mass balance is usually represented by a change of the equivalent water mass.

The computation especially for the direct gravitational attraction is sensitive to the location of the ice block relative to the position of the gravimeter. In order to keep computational accuracy, each of the elliptical glacier models was divided into 100 coaxial elliptical cylinders in the radial direction and each of these subcoaxial cylinders was divided into 100 blocks in the tangential direction. Related to

Table 5. Effect of sea-level changes on the displacement and gravity measurements at Ny-Ålesund. This table shows the sum of contributions from the two sea regions described in the text. The units of displacement and gravity are mm and μGal . Phase is relative to 1997 January 1.

Component	Secular Rate (per year)	Annual		Semi-annual	
		Amplitude	Phase	Amplitude	Phase
Vertical (+UP)	0.12	3.23	102.3	1.08	156.7
NS (+N)	0.00	0.01	38.0	0.01	215.5
EW (+E)	-0.01	0.14	-81.7	0.12	-26.8
Gravity	-0.04	1.18	101.4	0.39	161.6

the computation of gravity, it is evident that the area around the main base of Ny-Ålesund including the Ny-Ålesund Geodetic Observatory has not been covered with glacier during the past few decades, so we do not need to consider the effect of the Bouguer contribution from the underlying ice (Wahr *et al.* 1995). In the computation, we assumed that there are no glaciers within a small circular area of 1.5 arcmin in radius centred at the gravity station.

Results obtained using the Green's function for PREM earth model (Dziewonski & Anderson 1981) lead to 0.05 mm yr^{-1} , -0.83 mm yr^{-1} , and 2.04 mm yr^{-1} for the NS, EW and vertical displacements and to $-0.53 \mu\text{Gal yr}^{-1}$ for the gravity. For a check, we computed the gravity change using a Green's function only including the h_n term, and we obtained a value of $-0.628 \mu\text{Gal yr}^{-1}$ that is close to $-0.612 \mu\text{Gal yr}^{-1}$ estimated from the deformation rate of 2.04 mm yr^{-1} shown above and a free-air gradient of $-0.3 \mu\text{gal mm}^{-1}$. James & Ivins (1998) estimated the displacement and gravity changes in Antarctica driven by both the effects of past and present-day ice changes, and they give a ratio of $-0.27 \mu\text{Gal mm}^{-1}$ for the elastic response of the earth to PDIM basing on the similar Green's function formalism as here and the 1066B earth model of Gilbert & Dziewonski (1975). Our value is $-0.26 \mu\text{Gal mm}^{-1}$ (i.e. $-0.53/2.04$), which is similar in magnitude to their value, even though the spatial extent and the scale of ice sheets used in the respective computations are different.

3.4 Effects of PGR

3.4.1 Model and computation method

Based on three ice models, we have tested the sensitivity of our computation results to different ice models and upper mantle viscosity values. We tested three global ice models:

- (1) a model called ARC3+ANT4 described in the paper by Nakada & Okuno (2003), which is a model based on Nakada & Lambeck (1988, 1989) and Lambeck *et al.* (1990),
- (2) a model that combines model ANT4 and an ice model called here ANU, which is similar to the minimum ice model proposed by Lambeck (1995) and
- (3) ICE-3G (Tushingham & Peltier 1991).

Fig. 4 shows the comparison of the extent of ice in the North Europe, Siberia and Arctic regions at two epochs of the last glacial maximum (LGM), approximately 22 000 yr BP, and 12 000 yr BP. ARC3 includes all three of the Fennoscandian, Barents Sea and Kara Sea ice sheets. ICE-3G is a model modified from the prior model called ICE-2 (Wu & Peltier 1983) by adding the Barents Sea ice sheet, so that it can explain the history of the relative SL changes observed in Spitsbergen. This model is not so different from ARC3 in its spatial extent at LGM, but the history of ice melting is

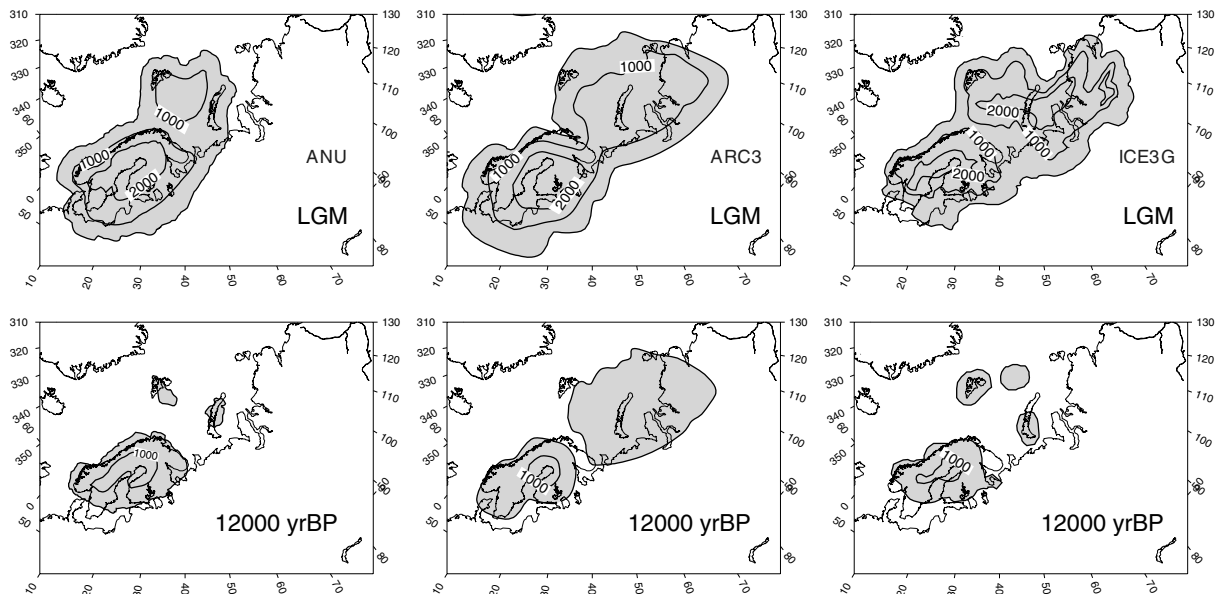


Figure 4. Extent and ice history of the three ice models in the Fennoscandian, Barents sea and Kara sea ice sheets, which were used for the sensitivity test. From the left, the ANU (Lambeck 1995), ARC3 (Lambeck *et al.* 1990) and ICE-3G (Tushingham & Peltier 1991) models are shown. Top: in the last glacial maximum (LGM) approximately 22 000 yr BP. Bottom: in 12 000 yr BP.

different. On the other hand, the melting history of the ANU model is quite different from that of the two other models. Thus, most of the ice sheets except for the Fennoscandian ice sheet have melted at 12 000 yr BP.

Our method of the PGR computation is similar to that described in Mitrovica & Peltier (1989), Mitrovica *et al.* (1994a) and James & Ivins (1998). We integrated the convolution of a viscoelastic Green's function defined at the Earth's perturbed surface and the past ice mass over its history of melting and the Earth's whole surface. We assumed here that the direct attraction term caused by the past ice mass is zero at the present. In a similar way to that described by Peltier (1974), the Green's function for a Maxwell earth model was computed using the viscoelastic load Love numbers extended from those for the elastic earth using the correspondence principle. Thus our computation results for gravity include the effect of the free-air contribution. On the timescale of PGR, the melting of the glaciers also affects the history of global SL change and these changes contribute to the history of PGR by changing the oceanic mass load on the Earth. The resultant eustatic SL rise is estimated to be as much as 120 m at most (for example, Nakada & Lambeck 1988). In this paper, we used a model for the history of SL changes that was proposed by Milne *et al.* (1999). The details of our computation method are described in Okuno & Nakada (2002).

The elastic structure and density profile inside the Earth are taken from the PREM model (Dziewonski & Anderson 1981). We computed the deformations and gravity changes up to the degree 180 in terms of spherical harmonics. For the Earth's viscosity model, referring to the studies by Nakada & Lambeck (1988), Okuno & Nakada (1999, 2001, 2002), and Nakada & Okuno (2003), we used 5×10^{20} Pa s and 1×10^{22} Pa s for the upper and lower mantle viscosities and 100 km for the lithospheric thickness as our base model for the computation of the PGR effect.

3.4.2 Computation results

Related to the PGR problem in the western Svalbard, referred to Maher *et al.* (1997), Kaufmann & Wu (1998) pointed out the possibility that a transition in the viscosity structure occurs in the direction from the Greenland deep-ocean basin to the shallow Barents Sea continental shelf. To examine the effect of uncertainty in the upper mantle viscosity, we have made a test by changing the upper mantle viscosity within the range 1×10^{20} Pa s and 1×10^{21} Pa s. In these tests, the lithosphere thickness and the lower mantle viscosity were fixed to 100 km and 1×10^{22} Pa s. Fig. 5 shows the results of the sensitivity test.

To examine the error in the computation of PGR effect, we compared our results with those of James & Lambert (1993) and Scherneck *et al.* (2002). Table 6 shows the comparison based on the ICE-3G model. The structural parameters used in each computation are also shown in Table 6. For the vertical component, our value is almost the same as that obtained by Scherneck *et al.* (2002), while our horizontal rates are close to rates of James & Lambert (1993). Thus, we may say that the computation error itself is less than 1 mm yr^{-1} for both the horizontal and vertical components when the computation is carried out using similar structural parameters and ice model. However, a point to be noted in Table 6 is that if we assume a 20 per cent larger value for the thickness (120 km), the vertical rate is reduced by about 40 per cent compared with the rate estimated using 100 km, but the EW component rate at Ny-Ålesund

is less sensitive to a change in lithosphere thickness within the range tested here.

As another check, we also compared our computation with the study by Wahr *et al.* (1995). These authors give a coefficient of $6.5 \text{ mm } \mu\text{Gal}^{-1}$, which represents the ratio of the viscous displacement to the viscous gravity change due to the effect of mass redistribution in the mantle. When we take into account the free-air gravity gradient, the coefficient of $6.5 \text{ mm } \mu\text{Gal}^{-1}$ leads to a value of $-0.146 \text{ } \mu\text{Gal mm}^{-1}$ (i.e. $-0.3+1/6.5$). If we take a mean value over two ice models (ARC3+ANT4 and for ICE-3G) and ten values of the upper mantle viscosities shown in Fig. 5, we obtain 1.50 mm yr^{-1} and $-0.22 \text{ } \mu\text{Gal yr}^{-1}$ for the vertical displacement and gravity rates, respectively, leading to a mean value of $-0.147 \text{ } \mu\text{Gal mm}^{-1}$, which is fully consistent with the value shown above.

4 DISCUSSION

Table 7 provides a summary of our comparison between the observed rates and the model computations. In this table, the scale rate error described in Section 2.1.2 is taken into account in the vertical rates from the GPS measurements.

4.1 Effect of SL changes

The estimated secular rate of the SL changes depends on the data length and the epoch of analysis as described in Section 2.4.2. The rate of the Ny-Ålesund tide gauge data for the recent 5 yr is about -18 mm yr^{-1} and it is about 5 times larger than the mean rate estimated from the 25 yr. Instead of -3.4 mm yr^{-1} used in Table 5, if we apply -15 mm yr^{-1} (i.e. mean of -18 mm yr^{-1} for Ny-Ålesund and -11 mm yr^{-1} for Barentsburg) to the inner circular area of 6° in radius, we obtain 0.48 mm yr^{-1} for the vertical displacement and $-0.08 \text{ } \mu\text{Gal yr}^{-1}$ for the gravity.

Another possible error source is an error due to the steric changes in the SL (i.e. SL change due to the sea surface temperature and the density of sea water). Therefore, the values shown in Table 5 may correspond to a maximum estimation. Sato *et al.* (2001b) estimated the effect of the annual sea surface height variability on superconducting gravity measurements, and they pointed out that ignoring the steric effect may cause an error of about 20–30 per cent in the estimation of the effect of sea surface height variations. However, all of our AG measurements were carried out in the same season (July–August) and therefore we can expect that any annual variations are substantially reduced. Compared to the gravity rate of $-2.5 \text{ } \mu\text{Gal yr}^{-1}$, the rate corrected for the effect of annual SL change shown in Table 7 differs only by $0.1 \text{ } \mu\text{Gal yr}^{-1}$. It corresponds to an error of 30 per cent in the estimation of the annual SL change and it can be safely ignored.

Table 7 and the error investigations mentioned above indicate that the effect of the SL changes with timescale of several decades around western Svalbard can be excluded as the major source of the discrepancy between the observed secular rates and the predictions.

4.2 Effect of PGR

4.2.1 Sensitivity of the horizontal components

As shown in Fig. 5, for the horizontal components at Ny-Ålesund, the two ice models (ARC3+ANT4 and ICE-3G) give a similar rate for

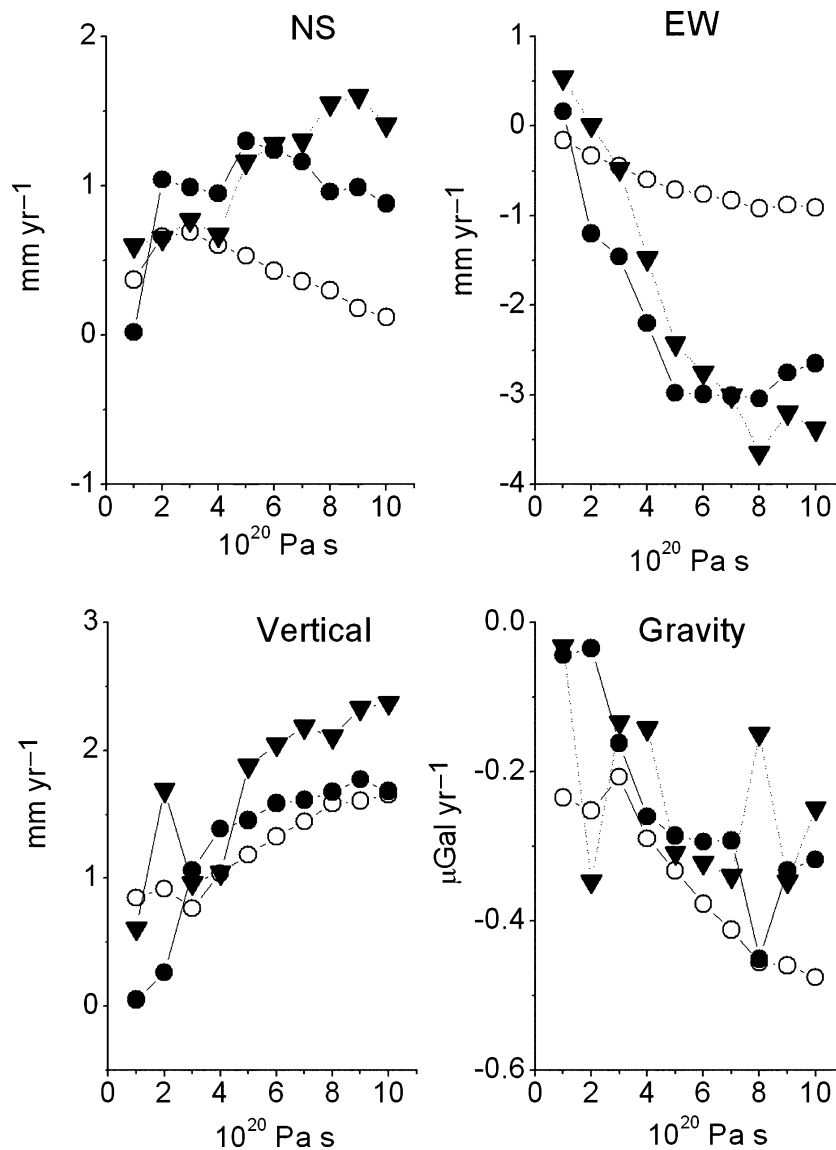


Figure 5. Sensitivity test of the computed PGR rates to the upper mantle viscosity. This figure shows the computation results obtained by assuming 1×10^{22} Pa s and 100 km for the lower mantle viscosity and the thickness of the lithosphere. The symbols are: filled circle, the ice model ARC3+ANT4 (Nakada & Lambeck 1988, 1989; Lambeck *et al.* 1990); open circle, ANU+ANT4 referred to Nakada & Lambeck (1989) and Lambeck (1995); and inverted triangle, ICE-3G (Tushingham & Peltier 1991).

Table 6. Comparison of the PGR displacement rates at Ny-Ålesund that were estimated using the ICE-3G model.

Mantle viscosity (Pa s)		Thickness (km)	Displacement rate (mm yr ⁻¹)			Author
Upper	Lower		NS	EW	Vertical	
1×10^{21}	2×10^{21}	120	0.5	-1.5	—	James & Lambert (1993)
1×10^{21}	2×10^{21}	120	0.12	-1.10	1.4	Scherneck <i>et al.</i> (2002)
1×10^{21}	2×10^{21}	120	0.52	-1.52	1.0	This study
1×10^{21}	2×10^{21}	100	0.38	-1.41	1.6	This study

both components of NS and EW components. However, compared to the two other models, the ANU model, which is a small ice model with a rapid melting history, shows a small horizontal rate in both components. Based on two different ice models of ICE-1 (Peltier & Andrews 1976) and ICE-3G, Mitrović *et al.* (1994b) carried out a similar test. They assumed 120 km, 1×10^{21} Pa s and 2×10^{21} Pa s

for the lithosphere thickness, the upper mantle and the lower mantle viscosities, respectively. According to their Fig. 5 for ICE-1 (a small ice model), the horizontal displacement rate around Ny-Ålesund is less than 0.8 mm yr^{-1} and 285 degrees in amplitude and azimuth angle measured from the north clockwise (i.e. less than 0.07 mm yr^{-1} and -0.8 mm yr^{-1} in terms of the displacement rates in the NS

Table 7. Comparison between the observed and predicted secular rates. The displacement rates are the rates relative to the NNR-NUVEL-1A model rates (see Table 1). GPS vertical rates have been corrected by a scale rate error of 1.6 mm yr^{-1} . The effect of present-day ice melting (PDIM) estimated by using -47 cm yr^{-1} as the rate of melting (see text) and using the SVAL model is shown in this table. For the PGR effect, this table shows the results estimated using a combination of structural parameters $5 \times 10^{20} \text{ Pa s}$ and 1×10^{22} for the upper and lower mantle viscosity and 100 km for the lithosphere thickness, which is our base model for the discussion.

		Displacement			Gravity
		NS	EW	Vertical	
		(mm yr^{-1})	(mm yr^{-1})	(mm yr^{-1})	($\mu\text{Gal yr}^{-1}$)
Observation	VLBI	0.2 (0.5)	-1.7 (0.5)	4.8 (1.1)	-2.5 (0.9)
	GPS (NYA1)	0.2 (0.6)	-2.3 (0.6)	4.8 (1.5)	
	GPS (NALL)	-0.1 (0.5)	-1.6 (0.5)	5.3 (0.9)	
	Tide gauge			5.2 (0.3)	
	Observation mean	0.1 (0.4)	-1.8 (0.4)	5.2 (0.6)	-2.5 (0.9)
Corrections					
1. RSL		0.00	-0.01	0.12	-0.04
2. PDIM	SVAL model	0.05	-0.83	2.04	-0.53
3. PGR	ARC3+ANT4	1.30	-2.98	1.46	-0.29
	ANU+ANT4	0.53	-0.71	1.18	-0.33
	ICE-3G	1.16	-2.43	1.88	-0.31
4. Sum of the corrections					
	ARC3+ANT4	1.35	-3.82	3.61	-0.84
	ANU+ANT4	0.58	-1.54	3.33	-0.88
	ICE-3G	1.21	-3.26	4.03	-0.86

and EW directions, respectively). On the other hand, their Fig. 3 for ICE-3G (a large ice model) indicates that the displacement rate at the same position is about 1.5 mm yr^{-1} and 302 degrees (i.e. 0.8 mm yr^{-1} and -1.3 mm yr^{-1} for the NS and EW directions, respectively). Therefore, we may say that a small ice model such as ICE-1 or ANU gives a small horizontal rate at Ny-Ålesund.

For the mantle viscosity in Svalbard Kaufmann & Wu (1998) examined the effect of lateral asthenospheric viscosity variations in the Barents Sea continental shelf by applying a finite element method. They tested an asthenospheric model where viscosity increases from 10^{18} Pa s to 10^{21} Pa s towards the Eurasian continent. The lower mantle viscosity is fixed to $1 \times 10^{21} \text{ Pa s}$ in their computation. They obtained a horizontal rate of 0.8 mm yr^{-1} in the northwest direction in northwest Svalbard. If we assume $2 \times 10^{20} \text{ Pa s}$ for the upper mantle viscosity that is lower than the nominal value of $5 \times 10^{20} \text{ Pa s}$, we obtain a rate of 1.6 mm yr^{-1} and 221° and 0.65 mm yr^{-1} and 89° in the amplitude and the azimuth angle for ARC3+ANT4 and ICE-3G, respectively. However, a similar small rate is obtained from the ANU model, even though we assume the nominal upper mantle viscosity value.

The sensitivity tests indicate that the horizontal displacement rates are sensitive to both the ice model and the viscosity of upper mantle. If we adjust the elastic rates to the observation mean values shown in Table 7, the expected viscous rates are estimated to be the order of $-0.2 \pm 0.4 \text{ mm yr}^{-1}$ and $-1.0 \pm 0.4 \text{ mm yr}^{-1}$ for the NS and EW components, respectively. Therefore, a small PGR rate obtained from the ANU model with the nominal upper mantle viscosity value (i.e. $5 \times 10^{20} \text{ Pa s}$) is not so different from the expected PGR rates in both the NS and EW components. On the other hand, if we take the large horizontal rates obtained from ARC3+ANT4 or ICE-3G, we must invoke another explanation. This will be discussed again in Section 4.2.3.

4.2.2 Sensitivity of the vertical components

For the vertical components, it is noticeable that any of three ice models compared here give a similar rate of $1.2\text{--}1.9 \text{ mm yr}^{-1}$ and

$-0.3 \mu\text{Gal yr}^{-1}$ with the nominal upper mantle viscosity value assumed in this study, although the three ice models differ in the spatial extent of the ice sheet and melting history.

By comparing the estimated elastic rates to the observed rates (i.e. a mean uplift rate of 5.2 mm yr^{-1} and a gravity rate of $-2.5 \mu\text{Gal yr}^{-1}$) shown in Table 7, viscous rates for the vertical components are estimated to be on the order of 3 mm yr^{-1} and $-1.9 \mu\text{Gal yr}^{-1}$. For both components, the computed vertical PGR rates are smaller than these expected values, even though we adopt a low upper mantle viscosity model or a small ice model, which can partly explain the discrepancy between the observed horizontal rates and the predicted ones.

4.2.3 A possible explanation

As described in the previous section, it is difficult to explain the observed high vertical rates by only the PGR effect. For the uplift rate in Svalbard, geological studies based on raised shore deposit give slightly larger contributions than the PGR effect shown in Table 7; for example, 3.3 mm yr^{-1} at Kvadehuksetta west of Ny-Ålesund (Hjelle 1993) and 2.8 mm yr^{-1} at Recherche Fjord south of Ny-Ålesund (Salvigsen 1976; Salvigsen *et al.* 1991). According to Fig. 6 of Lambeck (1996), southwestern Spitsbergen also suggests a higher uplift rate of about 3.1 mm yr^{-1} as a mean rate for the past 3000 yr. As pointed out by Blythe & Kleinspehn (1998), Hooke & Elverhoi (1996) and Fiedler & Faleide (1996), there is a possibility that massive erosion of Svalbard led to a mass redistribution that might enhance the PGR effects. The mean of these geological rates is 3.1 mm yr^{-1} . Adding this value to the predicted PDIM rate of 2.04 mm yr^{-1} for the nominal melting rate of -47 cm yr^{-1} gives a uplift rate of 5.1 mm yr^{-1} that is consistent with the observed rate of $5.2 \pm 0.6 \text{ mm yr}^{-1}$ shown in Table 7. For the gravity, if we apply the coefficient $-0.15 \mu\text{Gal mm}^{-1}$ derived from Wahr *et al.* (1995) to 3.1 mm yr^{-1} , we obtain $-0.47 \mu\text{Gal yr}^{-1}$. Using this value and the sum of the nominal SL and PDIM rates of $-0.57 \mu\text{Gal yr}^{-1}$ leads to a total rate of $-1.04 \mu\text{Gal yr}^{-1}$ that is slightly

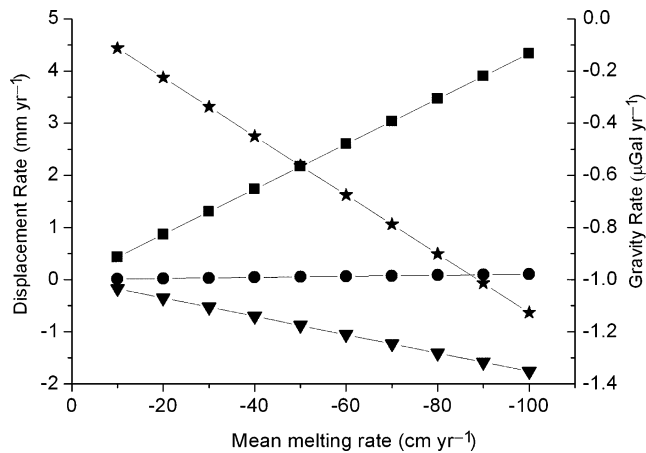


Figure 6. Variation in the PDIM effects as a function of the amplitude of melting rate. SVAL model is used for the computation. The symbols are: star, gravity (+downward force); square, radial displacement (+upward); circle, displacement in the NS component (+N) and inverted triangle, displacement in the EW component (+E).

larger than the total model rate ($-0.86 \mu\text{Gal yr}^{-1}$) shown in Table 7, although we must carefully examine the applicability of the rate of $-0.15 \mu\text{Gal mm}^{-1}$ to a problem including mass redistribution due to erosion.

The effect of PDIM is another candidate to explain the remaining discrepancy. Fig. 6 shows the variation in the estimated PDIM effects due to changing the rate of ice melting. To evaluate the agreement of model rates with observed rates, we plotted in Fig. 7 the gravity rates versus the corresponding vertical rates. Both PGR and PDIM model lines are shown in the plot. The slopes of these lines are $-0.15 \mu\text{Gal mm}^{-1}$ for PGR and $-0.26 \mu\text{Gal mm}^{-1}$ for PDIM, respectively. Here, the rate of $-0.26 \mu\text{Gal mm}^{-1}$ is the mean ratio of the gravity and displacement rates shown in Fig. 6. The crossing point of the PDIM and PGR model lines corresponds to the nominal ice melting rate of -47 cm yr^{-1} and upper mantle viscosity of $5 \times 10^{20} \text{ Pa s}$. As seen in Fig. 7, given the linear sensitivity shown in Fig. 6 of the PDIM model to ice melting rate, a clear way of improving the agreement between observed uplift rate and models is to increase the PDIM rate. Thus, we can explain most of the remaining discrepancy between the observed uplift rate and the expected PGR rate by assuming a larger melting rate of $70\text{--}80 \text{ cm yr}^{-1}$ than that assumed in this study. However, even if we assume this large PDIM rate, the expected sum of gravity rate is estimated to be at $-1.19 \mu\text{Gal yr}^{-1}$ (i.e. sum of -0.04 , -0.84 and -0.31 for the SL, PDIM and PGR effects), which is similar in magnitude to the value derived from the geological uplift rate mentioned above and is still about 1.6 times smaller than the observed rate.

As described above, the observed uplift rate may be explained from either the enhanced PGR rate or a larger PDIM rate or as an effect combining these two contributions. The horizontal rate may help to constrain our discussion. For example, for the EW component, which is sensitive to both the ice model and the upper mantle viscosity, the elastic loading effect is estimated to be -1.03 mm yr^{-1} , if we assume the PDIM rate of -75 cm yr^{-1} . By subtracting this value from the observed rate (i.e. -1.8 mm yr^{-1}), we obtain -0.77 mm yr^{-1} . Therefore, if we adopt our preferred value of $5 \times 10^{20} \text{ Pa s}$ for the upper mantle, we see that this value is close to -0.71 mm yr^{-1} that was obtained from a small ice model such as ANU+ANT4, although, as shown in Fig. 5, a large ice model can also take a small PGR rate of this order, if the upper mantle

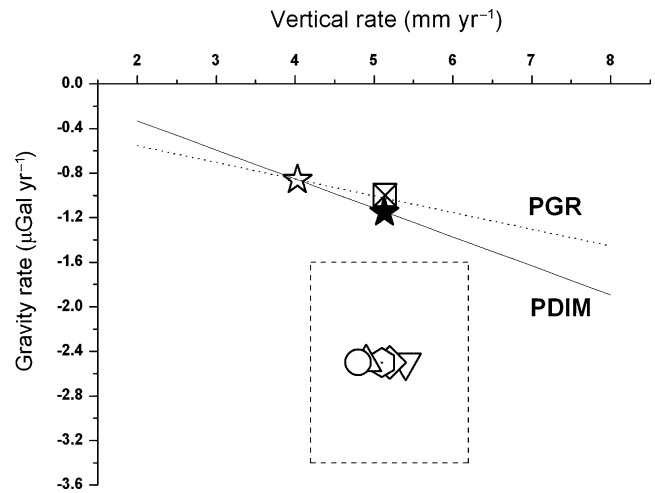


Figure 7. Comparison between the observed and model rates for the vertical components. Horizontal axis: vertical displacement rate in mm yr^{-1} , Vertical axis: gravity rate in $\mu\text{Gal yr}^{-1}$. The five geodetic observations VLBI (open circle), GPS NALL (open triangle), GPS NYA1 (inverted open triangle), Tide gauge (open diamond) and GPS Campaign (open hexagon) are plotted on a horizontal line corresponding to the observed gravity rate of $-2.5 \mu\text{Gal yr}^{-1}$. The rectangular region enclosed by the dashed lines shows the error box for the observations. The dotted line shows the gravity/vertical displacement ratio for viscous PGR effects ($-0.15 \mu\text{Gal mm}^{-1}$). The solid line shows the ratio for elastic PDIM effects ($-0.26 \mu\text{Gal mm}^{-1}$). The crossing of the two lines (open star) corresponds to the sum of the nominal SL, PDIM and PGR (ICE-3G) model contributions (refer to values used in Table 7). The filled star shows the position assuming a PDIM rate of -75 cm yr^{-1} and the nominal PGR rate. The open square with a cross mark shows the position assuming the nominal PDIM rate shown in Table 7 and a geological rate of 3.1 mm yr^{-1} and $-0.47 \mu\text{Gal yr}^{-1}$ as the corresponding PGR rate described in Section 4.2.3.

viscosity beneath the western Svalbard is $1 \times 10^{20} \text{ Pa s}$ to $2 \times 10^{20} \text{ Pa s}$. On this point, the NS component shows a tendency similar to the EW component. The PDIM rate of -75 cm yr^{-1} gives an elastic NS displacement rate of 0.08 mm yr^{-1} , and it leads to a viscous rate of -0.18 mm yr^{-1} (i.e. $-0.1\text{--}0.08$), which is close to the viscous rate of 0.53 mm yr^{-1} estimated from the small ice model rather than 1.16 mm yr^{-1} to 1.30 mm yr^{-1} estimated from the large ice models (see Table 7).

On the other hand, it is difficult to explain the observed high gravity rate by the three effects considered here including the enhanced geological rate mentioned above. In contrast to the gravity component, the reliability of the observed uplift rate is considered to be high, because the three different kinds of observation methods that are compared here, that is, VLBI, GPS (including the campaign data that cover more large area than that of the continuous observations) and tide gauge, give similar rates within their observation errors. In this context, a problem in our discussion is the observation error of the AG observations and the inferred gravity rate. As shown in Fig. 2 and described in Section 2.3.2, the error of AG measurements, which is the standard deviation of the hourly values during the observation period (usually a few days), is still large and, in addition, the measurements may suffer from systematic errors due to differences in the instruments that were used as shown for instance during inter-comparison campaigns at BIPM (Robertsson *et al.* 2001; Vitushkin *et al.* 2002). Therefore, more data points spanning a longer time period are needed in order to improve the reliability of the observed gravity rate and to tighten our discussion.

Due to both the observation errors and the ambiguity of the model predictions, it is not easy to conclude definitively whether a small ice model or a lower upper mantle viscosity better explains our geodetic data. A more careful examination may be required for the PGR effect, because, as we can see in Table 6, there is a trade-off between the magnitude of upper mantle viscosity and the thickness of lithosphere especially in the vertical displacement. In order to constrain the model computations more tightly, we need to increase the computation accuracy of the PGR effect. For the case of Svalbard, whose location is considered to be at an edge of the past ice sheet and which is an island, computation using a Green's function with much higher degree viscoelastic Love numbers (up to degree 1000 in a spherical harmonic decomposition) may be worthwhile to check the problem of the trade-off, but this is beyond the scope of the present study. However, we can at least say that increasing the accuracy of the PDIM computation and combining in the discussion the horizontal and vertical components are important to tighten the discussion of the PGR problem in Svalbard. The use of altimetry data from ICESat (Zwally *et al.* 2002, <http://icesat.gsfc.nasa.gov>) may help to improve the estimation accuracy of the PDIM effect.

Finally, for the displacement field in Europe, Marotta *et al.* (2004) recently discussed the combined effect of GIA (glacial isostatic adjustment) and tectonics on the displacement rates obtained from the dense GPS network in the central and northern Europe, in the region between 40 and 58 degrees in latitude. They claimed that the effect of tectonic deformations induced by the plate motion could not be ignored to explain the observation results for many European sites. However, according to their figures, in western Svalbard, the GIA effect is much more dominant than the tectonic effect.

5 CONCLUSIONS

The primary motivation of this study was to look for the origin of the difference in the uplift rates between the observations and those proposed in previous PGR studies. In addition, we tried also to explain complementary observations namely the horizontal displacement rates (GPS, VLBI) as well as the gravity rate (AG). We have investigated the following three effects: (1) SL change, (2) PDIM in Svalbard and (3) long-term regional displacement including the PGR effect.

For (1), the effect of SL change with a timescale of a few decades can be safely neglected as being the major origin of the discrepancy.

For (2), the effect of PDIM cannot be ignored in explaining consistently the mutual relations among the computed PGR effects and the observed secular rates for both the displacement and gravity. Our comparison between observed and predicted rates indicates that there is a possibility that the PDIM melting rate in Svalbard is more than 50 per cent larger than the rate of -47 cm yr^{-1} , which is the mean of glaciology-derived values over the Svalbard Archipelago. Such a melting rate would make it possible to explain the observed uplift seen by GPS and VLBI; however, the induced gravity rate would be too small (by roughly a factor 2) to be in agreement with the observed rate from absolute gravimetry. The geodetic measurements carried out at Ny-Ålesund are hence important to constrain not only the PGR rate but also the PDIM rate in Svalbard.

For (3), a rate of 3 mm yr^{-1} suggested from the geological data (i.e. mainly the shore line deposit data) can also reduce the discrepancy between the observed and the predicted vertical displacement rates. We have tested the sensitivity of the estimated PGR effects to the ice model and to the Earth's viscous parameters. The test indicates that the computation results for Ny-Ålesund are sensitive to

both the differences in the past ice models and the shallow viscous structure. In order to constrain the viscous structure, it is necessary to increase both the accuracies of the geodetic observations and the model predictions including the effect of PDIM.

ACKNOWLEDGMENTS

The authors thank Tonie van Dam for the discussions and comments about the data analysis especially for the AG measurements. Yoshiyuki Fujii provided useful suggestions for this study. We also thank Masao Nakada and Kurt Lambeck for their reading the draft manuscript. Comments from two reviewers were very helpful in improving the manuscript. The effort for transportation of equipment, installation and maintenance was relatively high for such a remote observation station as Ny-Ålesund. We acknowledge here the excellent support of the staff of Statens Kartverk and the local Kingsbay Kull Company. The observations were supported by several grants; the fund of European Commission under Contracts ERBFMGECT950065 and HPRI-CT-1999-00057; the fund of 'Application of Precise Satellite Positioning for Monitoring the Earth's Environment' of Special Co-ordination Funds for Promoting Science and Technology of the Ministry of Education, Culture, Sport, Science and Technology of Japan (MEXT). The SG observation was partly supported by National Grants in Aid of MEXT: No. 09NP1101, No. 13440135 and No. 1430132, and by Institute for Frontier Research on Earth Evolution organized at Japan Marine Science and Technology Center.

REFERENCES

- Altamimi, Z., Sillard, P. & Boucher, C., 2002. ITRF2000: a new release of the International Terrestrial Reference Frame for earth science applications, *J. geophys. Res.*, **107**(B10), 2214, ETG2-1-ETG2-19.
- Argus, D.F. & Gordon, R.G., 1996. Tests of the rigid-plate hypothesis and bounds on intraplate deformation using geodetic data from very long baseline interferometry, *J. geophys. Res.*, **101**, 13 555-13 572.
- Basnett, T.A. & Parker, D.E., 1997. Development of the Global Mean Sea Level Pressure Data Set GMSLP2. *Climatic Research Technical Note*, No.79. Hadley Centre, Meteorological Office, Bracknell, 16 pp. plus Appendices.
- Blythe, A.E. & Kleinspehn, K.L., 1998. Tectonically versus climatically derived Cenozoic exhumation of the Elasian plate margin, Svalbard: fission track analyses, *Tectonics*, **17**, 621-639.
- Bockmann, L., Grimstveit, L., Harsson, B.G., Kierulf, H.P., Kristiansen, O. & Plag, H.-P., 2002. Site surveys at the fundamental geodetic station in Ny-Ålesund, Svalbard, in *Proceedings of the NKG Meeting, October 1-4, 2002*, pp. 89-93, ed. Poutanen, M., Helsinki, Finish Geodetic Institute.
- Bos, M.S., Baker, T.F., Rothering, K. & Plag, H.-P., 2002. Testing ocean tide models in the Nordic seas with tidal gravity observations, *Geophys. J. Int.*, **150**, 687-694.
- Campbell, J. & Nothnagel, A., 2002. Vertical site motions in Europe—comparisons between techniques and with external data, in *Measurement of Vertical Crustal Motion in Europe by VLBI*, pp. 110-121, eds Campbell, J., Hass, R. & Nothnagel, A., Geodetic Institute, University of Bonn.
- Crossley, D. *et al.*, 1999. Network of superconducting gravimeters benefits a number of disciplines, *EOS, Trans. Am. geophys. Un.*, **80**(11), 121, 125-126.
- De Mets, C.P., Gordon, R.G., Argus, D.F. & Stein, S., 1994. Effect of recent revisions to the geomagnetic reversal time scale on estimates of current plate motions, *Geophys. Res. Lett.*, **21**, 2191-2194.

- Douglas, B.C., 1997. Global sea level rise: a redetermination, *Surv. Geophys.*, **18**, 279–292.
- Dowell, J. et al., 1997. The mass balance of circum-Arctic glaciers and recent climate change, *Quater. Res.*, **48**, 1–4.
- Dziewonski, A.D. & Anderson, D.L., 1981. Preliminary reference earth model, *Phys. Earth planet. Inter.*, **25**, 297–356.
- Farrell, W.E., 1972. Deformation of the Earth by surface loads, *Rev. Geophys.*, **10**, 751–797.
- Farrell, W.E., 1973. Earth tides, ocean tides and tidal loading, *Phil. Trans. R. Soc. Lond., A.*, **274**, 253–259.
- Fiedler, A. & Faleide, J.I., 1996. Cenozoic sedimentation along the south-western Barents Sea margin in relation to uplift and erosion of the shelf, *Glob. Planet. Change*, **12**, 75–93.
- Francis, O., Amalvict, M. & Hinderer, J., 1999. Intercomparison between the FG5#202 and FG5#206 at the site of the superconducting gravimeter C021 in Membach (Belgium), *Bull. Inf. BGI*, **84**, 36–39.
- Gilbert, F. & Dziewonski, A.M., 1975. An application of normal mode theory to the retrieval of structural parameters and source mechanisms from seismic spectra, *Phil. Trans. R. Soc.*, **278A**, 187–269.
- Hagedoorn, J.M. & Wolf, D., 2003. Pleistocene and Recent deglaciation in Svalbard: implications for tide-gauge, GPS and VLBI measurements, *J. Geodyn.*, **35**, 415–423.
- Hagen, J.O. & Liestol, O., 1990. Long-term glacier mass-balance investigations in Svalbard, 1950–88, *Annals of Glaciology*, **14**, 102–106.
- Heflin, M.B., 2004. GPS time series, <http://sideshow.jpl.nasa.gov/mbh/series.html/>.
- Hjelle, A., 1993. *Geology of Svalbard*, Polar handbook, No.7, Norwegian Polar Institute, 162 pp.
- Hooke, R.L. & Elverhoi, A., 1996. Sediment flux from a fjord during glacial period, Isfjorden, Spitsbergen, *Glob. Planet. Change*, **12**, 237–249.
- James, T.S. & Lambert, A., 1993. A comparison of VLBI data with the ICE-3G glacial rebound model, *Geophys. Res. Lett.*, **20**, 871–874.
- James, T.S. & Ivins, E.R., 1998. Predictions of Antarctic crustal motions derived by present-day ice sheet evolution and by isostatic memory of the Last Glacial Maximum, *J. geophys. Res.*, **103**(B3), 4993–5017.
- Kaufmann, G. & Wolf, D., 1996. Deglacial land emergence and lateral upper-mantle heterogeneity in the Svalbard Archipelago—II. Extended results for high-resolution load model, *Geophys. J. Int.*, **127**, 125–140.
- Kaufmann, G. & Wu, P., 1998. Lateral asthenospheric viscosity variations and post glacial rebound: a case study for the Barents Sea, *Geophys. Res. Lett.*, **25**(11), 1963–1966.
- Lambeck, K., Johnston, P. & Nakada, M., 1990. Holocene glacial rebound and sea-level change in NW Europe, *Geophys. J. Int.*, **103**, 451–468.
- Lambeck, K., 1995. Constraints on the Late Weichselian ice sheet over the Barents Sea from observations of raised shorelines, *Qua. Sci. Rev.*, **14**, 1–16.
- Lambeck, K., 1996. Limit on the areal extent of the Barents Sea ice sheet in Late Weichselian time, *Global and Planetary Change*, **12**, 41–51.
- Lambeck, K., Smither, C. & Ekman, M., 1998. Test of glacial rebound models for Fennoscandia based on instrumented sea- and lake-level records, *Geophys. J. Int.*, **135**, 375–387.
- Larson, K. & van Dam, T., 2000. Measuring Postglacial Rebound with GPS and Absolute Gravity, *Geophys. Res. Lett.*, **27**, 3925–3928.
- Ma, C., Sauber, J.M., Bell, L.J., Clark, T.A., Gordon, D., Himwich, W.E. & Ryan, J.W., 1990. Measurement of horizontal motions in Alaska using very long baseline interferometry, *J. geophys. Res.*, **95**(B13), 21 991–22 011.
- Macheret, Y.Y., Zhuravlev, A.B. & Borova, L.I., 1985. Thickness, subglacial relief and volume of Svalbard glaciers based on radio echo-sounding data, *Polar Geography and Geology*, **9**, 224–243.
- MacMillan, D.S., 2004. Rate difference between VLBI and GPS reference frame scales, *EOS Trans. Am. geophys. Un.*, **85**(47), Fall Meeting Suppl., Abstract G21B-05.
- Maher, H.D. Jr., Bergh, S., Braathen, A. & Ohta, Y., 1997. Svarfjella, Eidembukta and Daudmannsodden linearment: Tertiary orogen-parallel motion in crystalline hinterland of Spitsbergen's fold-thrust belt, *Tectonics*, **16**, 88–106.
- Marotta, A.M., Mitrovica, J.X., Sabadini, R. & Milne, G., 2004. Combined effects of tectonics and glacial isostatic adjustment on interplate deformation in central and northern Europe: Application to geodetic baseline analyses, *J. geophys. Res.*, **109**(B01413), doi:10.1029/2002JB002337.
- McCarthy, D.D., 1996. IERS Conventions 1996, *IERS Tech. Note*, **21**, Paris.
- Milne, G.A., Mitrovica, J.X. & Davis, J.L., 1999. Near-field hydro-isostasy: the implementation of a revised sea-level equation, *Geophys. J. Int.*, **139**, 464–482.
- Mitrovica, J.X. & Peltier, W.R., 1989. Pleistocene deglaciation and the global gravity field, *J. geophys. Res.*, **94**, 13 651–13 671.
- Mitrovica, J.X., Davis, J.L. & Shapiro, I.I., 1994a. A spectral formalism for computing three-dimensional deformations due to surface loads, 1. Theory, *J. geophys. Res.*, **99**(B4), 7057–7073.
- Mitrovica, J.X., Davis, J.L. & Shapiro, I.I., 1994b. A spectral formalism for computing three-dimensional deformations due to surface loads, 2. Present-day glacial isostatic adjustment, *J. geophys. Res.*, **99**(B4), 7075–7101.
- Nakada, M. & Lambeck, K., 1988. The melting history of the Late Pleistocene Antarctic ice sheet, *Nature*, **333**, 36–40.
- Nakada, M. & Lambeck, K., 1989. Late Pleistocene and Holocene sea-level changes in Australian region and mantle rheology, *Geophys. J.*, **96**, 497–517.
- Nakada, M. & Okuno, J., 2003. Perturbations of the Earth's rotation and their implementations for the present-day mass balance of both polar ice caps, *Geophys. J. Int.*, **152**, 124–138.
- Okuno, J. & Nakada, M., 1999. Total volume and temporal variation of meltwater from last glacial maximum inferred from sea-level observations at Barbados and Tahiti, *PALAEO*, **146**, 283–293.
- Okuno, J. & Nakada, M., 2001. Effect of water load on geophysical signals due to glacial rebound and implications for mantle viscosity, *Earth Planets Space*, **53**, 1121–1135.
- Okuno, J. & Nakada, M., 2002. Contributions of ineffective ice load on sea-level and free-air gravity, ice sheet, sea level and the dynamic earth, *Geodynamics Series 29*, Am. Geophys. Un., 177–185.
- Peltier, W.R., 1974. Impulse response of a Maxwell Earth, *Rev. Geophys.*, **12**, 649–669.
- Peltier, W.R. & Andrews, J.T., 1976. Glacial Isostatic Adjustment, I. The forward problem, *Geophys. J. R. astr. Soc.*, **46**, 605–646.
- Plag, H.-P., 1999. Measurements of vertical crustal motion in Europe by VLBI -Station report for Ny-Ålesund, Norwegian Mapping Authority, *Proceed. 13-th Working Meeting of European VLBI for Geodesy and Astrometry*, eds. W. Schlüter and R. Hass, BKG, Frankfurt, Germany, 65–77.
- Plag, H.-P. & Tsimplis, N.M., 1999. Temporal variability of the seasonal sea-level cycle in North Sea and Baltic Sea in relation to climate variability, *Global and Planetary Change*, **20**, 173–203.
- Plag, H.-P. & Gueguen, E., 2002. Geophysical Interpretation -Part 1: Northern Europe, in *Measurement of Vertical Crustal Motion in Europe by VLBI*, pp. 125–132, eds Campbell, J., Haas, R. & Nothnagel, A.
- Robertsson, L. et al., 2001. Results from the Fifth International Comparison of Absolute Gravimeters, ICAG97, *Metrologia*, **38**, 71–78.
- Rodwell, M.J., Rowell, D.P. & Folland, C.K., 1999. Oceanic forcing of the wintertime North Atlantic Oscillation, *Nature*, **398**, 320–323.
- Salvigsen, O., 1976. Radiocarbon dating and the extension of the Weichselian ice-sheet in Svalbard, *Norsk Polarinst. Aarb.*, 209–224.
- Salvigsen, O., Elgersma, A. & Landvik, J.Y., 1991. Radiocarbon dating raised beach in northwestern Wedel Jarlsberg Land, Spitsbergen, Svalbard, *Wypzr. Geogr. Na Spitsbergen, UMCS, Lublin*, 9–16.
- Sato, T. & Hanada, H., 1984. A program for the computation of oceanic tidal loading effects 'GOTIC', *Proc. Int. Conf. Earth Rotation and Terrest. Refer. Frame*, 742–747.
- Sato, T. et al., 2001a. Continuous gravity observation at Ny-Ålesund, Svalbard, Norway with a superconducting gravimeter CT#039, *J. Geodetic Soc. Japan*, **47**(1), 341–345.
- Sato, T., Fukuda, Y., Aoyama, Y., McQueen, H., Shibuya, K., Tamura, Y., Asari, K. & Ooe, M., 2001b. On the observed annual gravity variation

- and the effect of sea surface height variations, *Phys. Earth planet. Inter.*, **123**, 45–63.
- Sato, T., Tamura, Y., Matsumoto, K., Asari, K., Plag, H.-P., van Dam, T. & Francis, O., 2003. Comparison between modeled and observed gravity tidal parameters at Ny-Ålesund, Svalbard, in *Proceedings of the Workshop: IMG-2002 in Luxemburg*, pp. 143–148, eds Francis, O. & van Dam, T.
- Scherneck, H.-G., Haas, R. & Bos, M.S., 2002. Station motion model, northern Europe, in *Measurement of Vertical Crustal Motion in Europe by VLBI*, pp. 30–50, eds Campbell, J., Haas, R. & Nothnagel, A., Geodetic Institute, University of Bonn.
- Steinforth, C., Hass, R., Lidberg, M. & Nothnagel, A., 2003. Stability of Space Geodetic Reference Points at Ny-Ålesund and Their Eccentricity Vectors, in *Proceedings of Working Meeting on European VLBI for Geodesy and Astrometry*, held at Leipzig, May 9–10, 2003, eds Schwegmann, W. & Thorandt, V., 83–89, Bundesamt für Kartographie und Geodäsie, Frankfurt/Leipzig.
- Tamura, Y., Sato, T., Ooe, M. & Ishiguro, M., 1991. A procedure for tidal analysis with a Bayesian information criterion, *Geophys. J. Int.*, **104**, 507–516.
- Tushingham, A.M. & Peltier, W.R., 1991. ICE-3G: a new global model of Late Pleistocene deglaciation based upon geophysical predictions of postglacial relative sea level change, *J. geophys. Res.*, **96**, 4497–4523.
- van Dam, T., Larson, K., Wahr, J., Gross, S. & Olivier, F., 2000. Using GPS and Gravity to Infer Ice Mass Changes in Greenland, *EOS, Trans. Am. geophys. Un.*, **81**(37), 424, 426–427.
- Vitushkin, L. *et al.*, 2002. Results of the Sixth International Comparison of Absolute Gravimeters, ICAG-2001, *Metrologia*, **39**(5), 407–424.
- Wahr, J., 1985. Deformation Induced by Polar Motion, *J. geophys. Res.*, **90**(B11), 9363–9368.
- Wahr, J., DaZhong, H. & Trupin, A., 1995. Predictions of vertical uplift caused by changing polar ice volumes on a viscoelastic earth, *Geophys. Res. Lett.*, **22**(8), 977–980.
- World Glacier Monitoring Service, 1989. *World Glacier Inventory Status 1988*, eds Haerberli, W., Bösch, H., Scherler, K., Østrem, G. & Wallén, C.C., Zürich, Switzerland.
- World Glacier Monitoring Service, 1998. *Fluctuations of Glaciers 1990–1995*, eds Haerberli, W., Hoelzle, M., Suter, S. & Frauenfelder, R., Zürich, Switzerland.
- World Glacier Monitoring Service, 2001. *Glacier Mass Balance Bulletin No. 6 (1998–1999)*, eds Haerberli, W., Frauenfelder, R. & Hoelzle, M., Zürich, Switzerland.
- Woodworth, P.L., 1991. The Permanent Service for Mean Sea Level and the Global Sea Level Observing System. *Journal of Coastal Research*, **7**, 699–710.
- Woodworth, P.L., Tsimplis, M.N., Plather, R.A. & Shennan, I., 1999. A review of the trends observed in British Isles mean sea level data measured by tide gauge. *Geophys. J. Int.*, **136**, 651–670.
- Wu, P. & Peltier, W.R., 1983. Glacial isostatic adjustment and free air gravity anomaly as a constraint on deep mantle viscosity, *Geophys. J. R. astr. Soc.*, **74**, 377–450.
- Zwally, H.J., Shutz, B., Abdalati, W., Palm, J., Spinhirne, J. & Thomas, R., 2002. ICESat's Laser Measurements of Polar Ice, Atmosphere, Ocean, and Land, *J. Geodyn.*, **34**(3–4), 405–445.